Cell Calcium xxx (2016) xxx–xxx

Contents lists available at ScienceDirect

Cell Calcium

journal homepage: www.elsevier.com/locate/ceca

Cytoskeleton rotation relocates mitochondria to the immunological synapse and increases calcium signals

Ilaria Maccari[a,1], Renping Zhao[b], Martin Peglow[a], Karsten Schwarz[a], Ivan Hornak[a], Mathias Pasche[c,2], Ariel Quintana[b,3], Markus Hoth[b,*], Bin Qu[b], Heiko Rieger[a,*]

[a] Theoretical Physics, Saarland University, 66041 Saarbrücken, Germany
[b] Biophysics, Center for Integrative Physiology and Molecular Medicine (CIPMM), School of Medicine, Saarland University, 66421 Homburg, Germany
[c] Physiology, Center for Integrative Physiology and Molecular Medicine (CIPMM), School of Medicine, Saarland University, 66421 Homburg, Germany

ARTICLE INFO

Article history:
Received 20 May 2016
Received in revised form 24 June 2016
Accepted 24 June 2016
Available online xxx

Keywords:
Mitochondria
CRAC channels
Orai channels
Plasma membrane calcium ATPase (PMCA)
Immunological synapse (IS)
Rotation model

ABSTRACT

Ca^{2+} microdomains and spatially resolved Ca^{2+} signals are highly relevant for cell function. In T cells, local Ca^{2+} signaling at the immunological synapse (IS) is required for downstream effector functions. We present experimental evidence that the relocation of the MTOC towards the IS during polarization drags mitochondria along with the microtubule network. From time-lapse fluorescence microscopy we conclude that mitochondria rotate together with the cytoskeleton towards the IS. We hypothesize that this movement of mitochondria towards the IS together with their functionality of absorption and spatial redistribution of Ca^{2+} is sufficient to significantly increase the cytosolic Ca^{2+} concentration. To test this hypothesis we developed a whole cell model for Ca^{2+} homoeostasis involving specific geometries for mitochondria and use the model to calculate the spatial distribution of Ca^{2+} concentrations within the cell body as a function of the rotation angle and the distance from the IS. We find that an inhomogeneous distribution of PMCA pumps on the cell membrane, in particular an accumulation of PMCA at the IS, increases the global Ca^{2+} concentration and decreases the local Ca^{2+} concentration at the IS with decreasing distance of the MTOC from the IS. Unexpectedly, a change of CRAC/Orai activity is not required to explain the observed Ca^{2+} changes. We conclude that rotation-driven relocation of the MTOC towards the IS together with an accumulation of PMCA pumps at the IS are sufficient to control the observed Ca^{2+} dynamics in T-cells during polarization.

© 2016 Elsevier Ltd. All rights reserved.

1. Introduction

Organelle polarization is a fundamental biological process for many cellular functions [1–5]. Cytotoxic T lymphocytes (CTL) and natural killer (NK) cells are highly polarized during cell migration and immunological synapse (IS) formation with their cognate target cells like tumor cells or virus infected cells [6–8]. Polarity is often controlled by actin polymerization induced by Cdc42 [9] or Arp2/3-dependent actin nucleation [10]. The specificity of target cell killing is, among other mechanisms, guaranteed through polarized secretion of lytic granules (LG) containing perforin and granzymes at the IS [11–13]. The microtubule organizing center (MTOC, centrosome) is a key organelle involved in repositioning of LG towards the IS following actin depletion [14], and secretion of LG at the IS is one of the central polarization steps in CTL and NK cells [4,15]. The MTOC moves to the IS within several minutes of IS formation [13,16]. This directed movement requires the motor protein dynein [17] which according to the favored mechanism, mediates MTOC repositioning to the IS by generating force through microtubule binding at the outer ring of actin at the IS. This process is also referred to as cortical sliding mechanism. This view has recently been challenged by Yi et al. [18] who present a series of experiments favoring a mechanism that dynein mediates MTOC repositioning through a "microtubule end-on capture-shrinkage mechanism", by which dyneins act on microtubules docked at the center of the IS and not at the outer actin ring. Regardless of the model, the MTOC is considered a master regulator of T cell polarization [17] and it is most

* Corresponding authors.
E-mail addresses: markus.hoth@uks.eu (M. Hoth), h.rieger@mx.uni-saarland.de (H. Rieger).
[1] Present address: Physics Department, "La Sapienza" University of Rome, 00185 Rome, Italy.
[2] Present address: MRC Laboratory for Molecular Biology, Cambridge CB2 0QH, England, UK.
[3] Present address: Division of Signalling and Gene Expression, La Jolla Institute for Allergy and Immunology, La Jolla, CA 92037, United States.

http://dx.doi.org/10.1016/j.ceca.2016.06.007
0143-4160/© 2016 Elsevier Ltd. All rights reserved.

Please cite this article in press as: I. Maccari, et al., Cytoskeleton rotation relocates mitochondria to the immunological synapse and increases calcium signals, Cell Calcium (2016), http://dx.doi.org/10.1016/j.ceca.2016.06.007

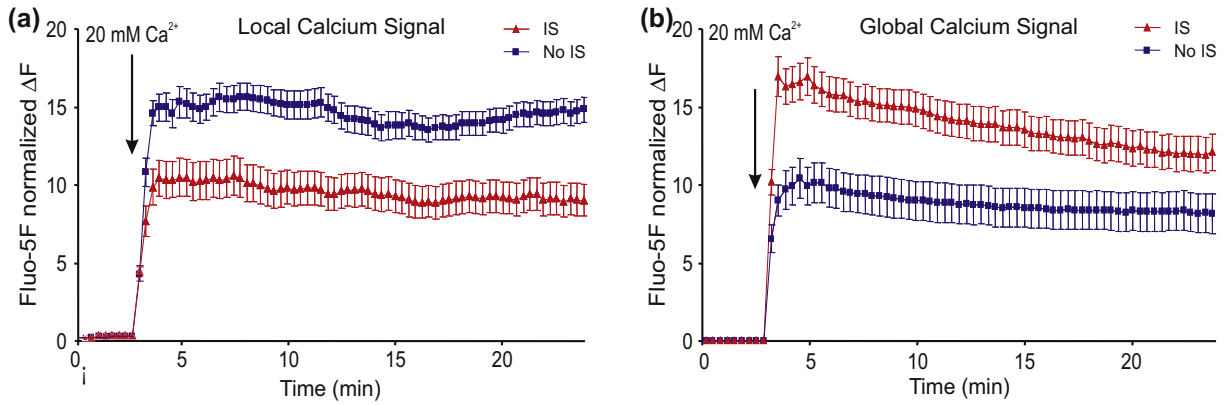

Fig. 1. Mitochondrial localization at the IS modulates local and global Ca^{2+} levels. Fluo-5F/AM loaded Jurkat E6.1 T-cells were settled either on anti-CD3 antibody-coated coverslips (inducing IS formation) or on poly-L-ornithine-coated coverslips (no IS formation). Ca^{2+} stores were depleted by 5–7 min thapsigarin (1 μM) pre-treatment in Ca^{2+} free solution and subsequently, cells were exposed to 20 mM Ca^{2+}. **(a)** Mean normalized fluorescence of Fluo-5F by TIRFM of 33 (with IS formation, red trace) and 37 (no IS formation, blue trace) cells over time (at 20 min, $p < 0.0001$) representing local Ca^{2+} signals at the plasma membrane. **(b)** Mean normalized fluorescence of Fluo-5F by epifluorescence microscopy of 17 (with IS formation, red trace) and 18 (no IS formation, blue trace) cells over time (at 20 min, $p = 0.036$) representing global Ca^{2+} signals. (For interpretation of the references to color in this figure legend, the reader is referred to the web version of this article.)

likely guiding other organelles like the Golgi apparatus [19,20], mitochondria [21–24] and LG [13] to the IS.

Several of the signaling steps governing CTL and/or NK cell dependent target cell death are Ca^{2+} dependent: (1) MTOC relocalization to the IS [18]; (2) mitochondria relocalization to the IS [24,25]; (3) secretion of LG at the IS [26–28]; (4) perforin-dependent lysis of target cells [29]. While the exact molecular mechanisms of how Ca^{2+} is involved in regulating these processes are not resolved yet, it is clear that Ca^{2+} influx through Orai (mostly Orai1) channels is the main Ca^{2+} source [28,30,31]. Ca^{2+} influx at the IS through Orai1 channels is among other factors controlled by mitochondrial positioning at the IS. There, mitochondria act as Ca^{2+} sinks, whereby they control Ca^{2+} dependent activity of Orai channels and local Ca^{2+} concentrations at the IS as well as global cytosol Ca^{2+} concentrations ($[Ca^{2+}]_{cyt}$) [23,32,33].

In this paper we show that cytoskeleton rotation relocates mitochondria to the immunological synapse. Unexpectedly, repositioning of mitochondria alone can modulate the global cytosolic Ca^{2+} concentration, independent of any influence of mitochondrial position on CRAC/Orai channel activity. We determine the geometric path that mitochondria take during relocation towards the IS and show that it is correlated with a rotation of the MTOC and microtubular network. We implement this rotation into a model for spatiotemporal Ca^{2+} dynamics in T-cells that we proposed recently [33] and present the predictions of this model about the dependence of the global and local Ca^{2+} concentration on the rotation angle of the cytoskeleton/mitochondria system.

2. Results

2.1. Mitochondria relocation correlates with Ca^{2+} increase

In 2011, we have shown that mitochondrial relocation to the IS decreases local cytosolic Ca^{2+} levels but increases global ones [23]. We confirm these findings by an independent set of experiments in human Jurkat T-cells (Fig. 1) similar to the experiments shown in Fig. 4C and D of our previous publication [23]. In case an IS is induced by anti-CD3 antibodies on the coverslip, mitochondria localize to the IS as shown by Quintana et al. [23] and the local Ca^{2+} signals at the plasma membrane are lower compared to conditions in which no IS was formed (Fig. 1a). In contrast the global Ca^{2+} signals are higher in case of IS formation (Fig. 1b). Localization of mitochondria at the IS thus decreases the local Ca^{2+} levels compared to experiments where no IS is formed but increases the global ones. In conclusion mitochondrial localization relative to CRAC channels at the IS determines local and global Ca^{2+} concentrations.

2.2. Mitochondria relocation correlates with cytoskeleton movement

Whereas it is undisputed that mitochondria relocalize to the IS, the exact mechanisms of the relocalization process have not been resolved. Mitochondrial fusion/fission [21] and cytoskeletal reorganization are very likely involved [3,5] but the exact mechanisms are not understood. Considering the MTOC relocalization to the IS [13,16,19,20] and its potential to guide other organelles there, it is reasonable to assume that the MTOC and mitochondrial movement could be correlated. We thus tested the hypothesis that mitochondria translocation and microtubule network reorientation towards the IS are correlated. We fluorescently labeled microtubules (with EMTB-3 × GFP) and mitochondria (with MitoTracker or DsRed2-Mito-7) in CTL. CTL were conjugated with target cells at 37 °C and translocation of microtubule network and mitochondria was visualized by time lapse microscopy. We found that mitochondrial localization was closely associated with microtubules (Fig. 2a). Following contact between CTL and a target cell, mitochondria were passively translocated to the IS along with microtubule network reorientation (Fig. 2a and Supplementary Movie 1). Moreover, we observed that occasionally mitochondria could actively move along microtubule tracks (Fig. 2b and Supplementary Movie 2). These results show that mitochondria relocation correlates with cytoskeleton rearrangement, especially microtubule network reorientation towards the IS.

2.3. Quantitative analysis of cytoskeleton and mitochondria rotation

For each time frame we extracted the three-dimensional positions of the MTOC, the IS, the cell center, and individual mitochondria using a higher time resolution for 3D pictures as described in the Materials and Methods section. The position data for all objects in a single frame were brought into a standard coordinate system by two rotations and one translation, such that MTOC, IS, and cell center lie in one plane, the x-z plane, and the rotation axis is parallel along the y-axis. We assume that the MTOC (in this case located at 90°) moves towards the IS. In Fig. 3a we sketch the movement of mitochondria that one expects in case mitochondria are attached to the microtubules: in the right half space they are rotated

Please cite this article in press as: I. Maccari, et al., Cytoskeleton rotation relocates mitochondria to the immunological synapse and increases calcium signals, Cell Calcium (2016), http://dx.doi.org/10.1016/j.ceca.2016.06.007

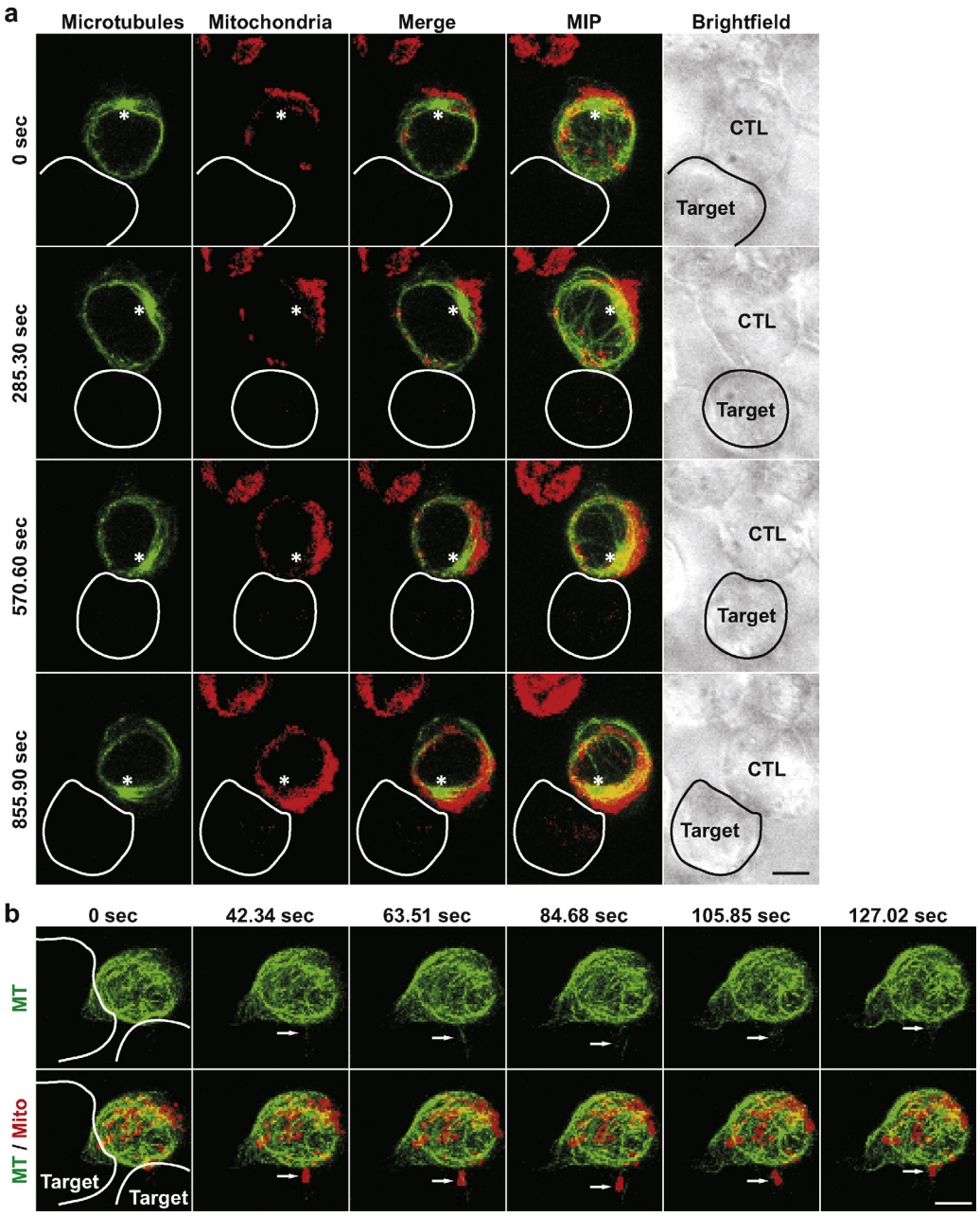

Fig. 2. Microtubules and mitochondria rotate together towards the IS during polarization. CTL were conjugated with SEA/SEB-pulsed Raji cells (target). **(a)** Mitochondria are translocated along with microtubule network. Microtubules and mitochondria were labeled by EMTB-3 × GFP and MitoTracker Deep Red, respectively. The time lapse was taken at 37 °C every 21.17 s by a confocal microscope with a 63×objective. MTOC is marked by the asterisk. MIP: maximum intensity projection. **(b)** Mitochondria can be actively transported along microtubules. Microtubules and mitochondria were labeled by EMTB-3 × GFP and DsRed2-Mito-7. The time lapse was taken at 37 °C every 19.02 s by a confocal microscope with a 63× objective. The maximum intensity projections are shown. Arrowheads highlight the transported mitochondrion and the corresponding microtubule. Scale bars are 5 μm.

towards the IS, in the left half space they are rotated away from it. Consequently vectors pointing from the center to mitochondria on the right half space decrease their angle with the vector from the center to the IS in the same way as the vector pointing from the center to the MTOC. In the left half space the mitochondria angles increase.

In Fig. 3b we show a histogram for the mitochondria angles extracted from tracking data acquired with a spinning disk confocal microscope (see Materials & Methods), in which CTL were settled on CD3/CD28 antibody-coated coverslips and IS was formed between CTL and coverslips. We analyzed two time points: before (at 0 s) and after polarization (at 186 s). Compared to the angles before polarization, the distribution after polarization is systematically shifted to the lower angles as expected from a rotation. The histogram for the mitochondria angles in the left half space is shown in Fig. 3c: here the angles after polarization are systematically shifted to larger values as expected from a rotation. In conclusion, a correlated rotation model of MTOC and the microtubules with attached mitochondria explains the observed mitochondria movement during IS formation very well.

The number of mitochondria data points in the left half space (Fig. 3c) is much smaller than the number of data points in the right half space (Fig. 3b). The reason is a displacement of microtubules from the left into the right half space during the repositioning of the MTOC as is clearly visible in Fig. 5A of Ref. [18]. This displacement is mechanically plausible: When microtubules are caught by

Please cite this article in press as: I. Maccari, et al., Cytoskeleton rotation relocates mitochondria to the immunological synapse and increases calcium signals, Cell Calcium (2016), http://dx.doi.org/10.1016/j.ceca.2016.06.007

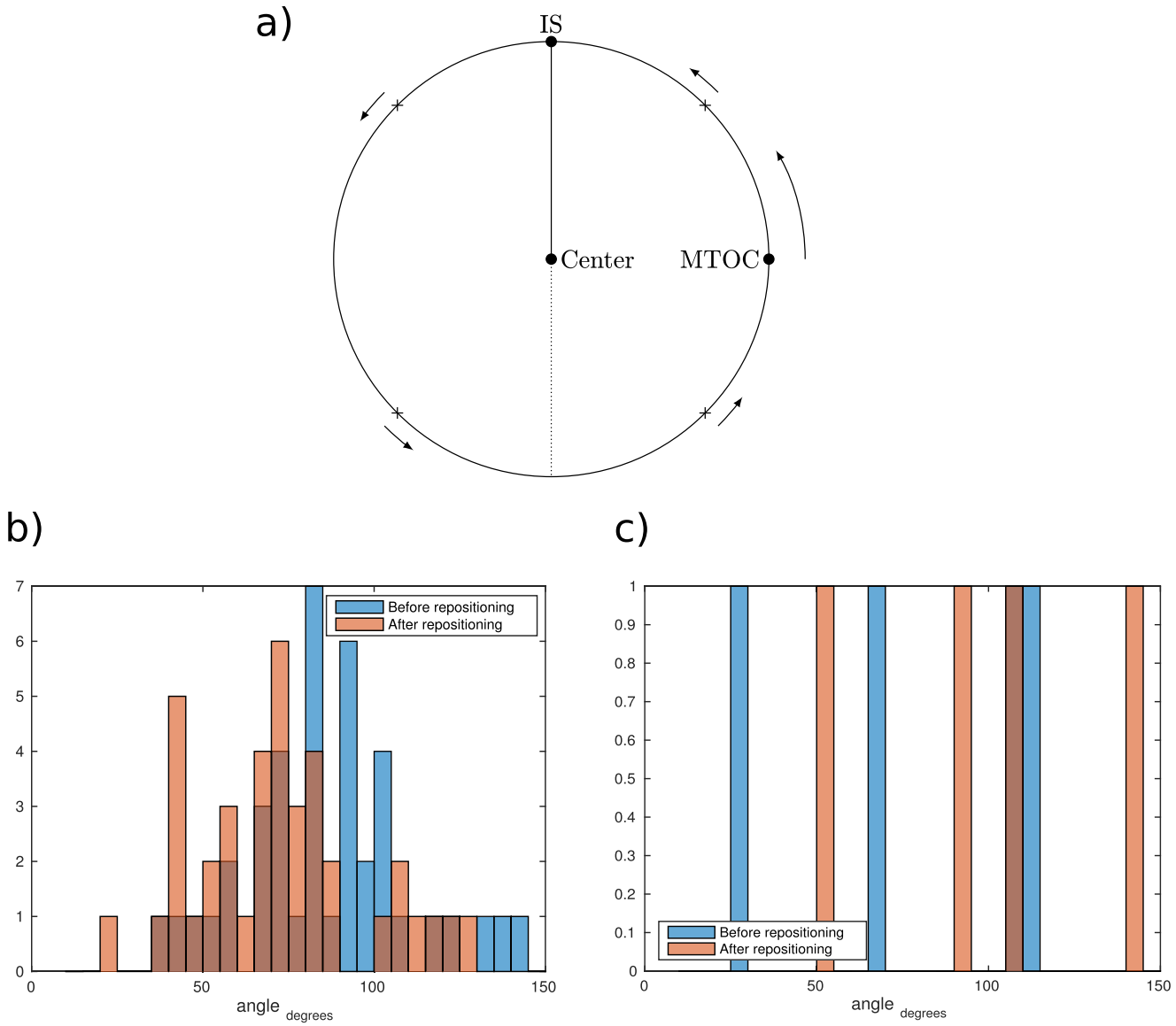

Fig. 3. Rotation angle of mitochondria increases during polarization. **(a)** Sketch of the rotational movement of MTOC and mitochondria in the plane perpendicular to the rotation axis. Mitochondria in the right half space rotate towards the IS, mitochondria in the left half space rotate away from the IS. **(b)** Histogram of the rotation angle of mitochondria in the right half plane at the beginning and the end of the polarization. Acquisitions from spinning disk confocal were analyzed. **(c)** Same as (b) for the left half space.

dynein, they are pulled towards the IS, and, consequently, the whole structure of microtubules and MTOC is repositioned. This movement is opposed by friction of the solvent in the cell that push microtubules in direction opposed to the movement. Microtubules caught by dynein have fixed position, but the position of the other microtubules relative to cytoskeleton change, and the microtubule structure "opens" in the direction towards IS as observable in Fig. 5A of Ref. [18].

2.4. Mathematical modeling reveals the mechanism for experimentally observed Ca^{2+} increase during polarization

We hypothesize that the observed changes in local and global Ca^{2+} concentration are intimately connected to the observed rotational relocation of the mitochondria towards the IS and that the underlying mechanism is the spatial rearrangement of Ca^{2+} sources, sinks and compartments during the observed mitochondrial movement. To test this, we formulated a mathematical three-dimensional (3D) model for the spatiotemporal distribution of Ca^{2+} in the cell cytosol, the mitochondria and the ER as a function of the geometry and spatial arrangement of mitochondria within the cell, as we have observed them experimentally.

Our 3D full cell Ca^{2+} model assumes a spherical cell with a concentric nucleus and a spindle-like arrangement of thin, cylindrical mitochondria compartments between nucleus and plasma membrane (see Figs. 4a and 5a for a sketch). The spindle-like arrangement is motivated by the spindle formed by microtubules emanating from a MTOC, c.f. Fig. 2a and [18], and the observation that mitochondria are predominantly attached to microtubules and form filamentous structures [34,35]. The whole spindle can be rotated around an arbitrary axis by a specific angle, with zero angle corresponding to the configuration when the spindle center and the center of the IS match. The IS is defined as a small circular region at the north pole of the sphere.

The compartments can exchange Ca^{2+} through the compartment boundaries via channels and pumps which are distributed homogeneously or in-homogeneously over the compartment surfaces, defined quantitatively as Ca^{2+} flux per area. CRAC channels

Please cite this article in press as: I. Maccari, et al., Cytoskeleton rotation relocates mitochondria to the immunological synapse and increases calcium signals, Cell Calcium (2016), http://dx.doi.org/10.1016/j.ceca.2016.06.007

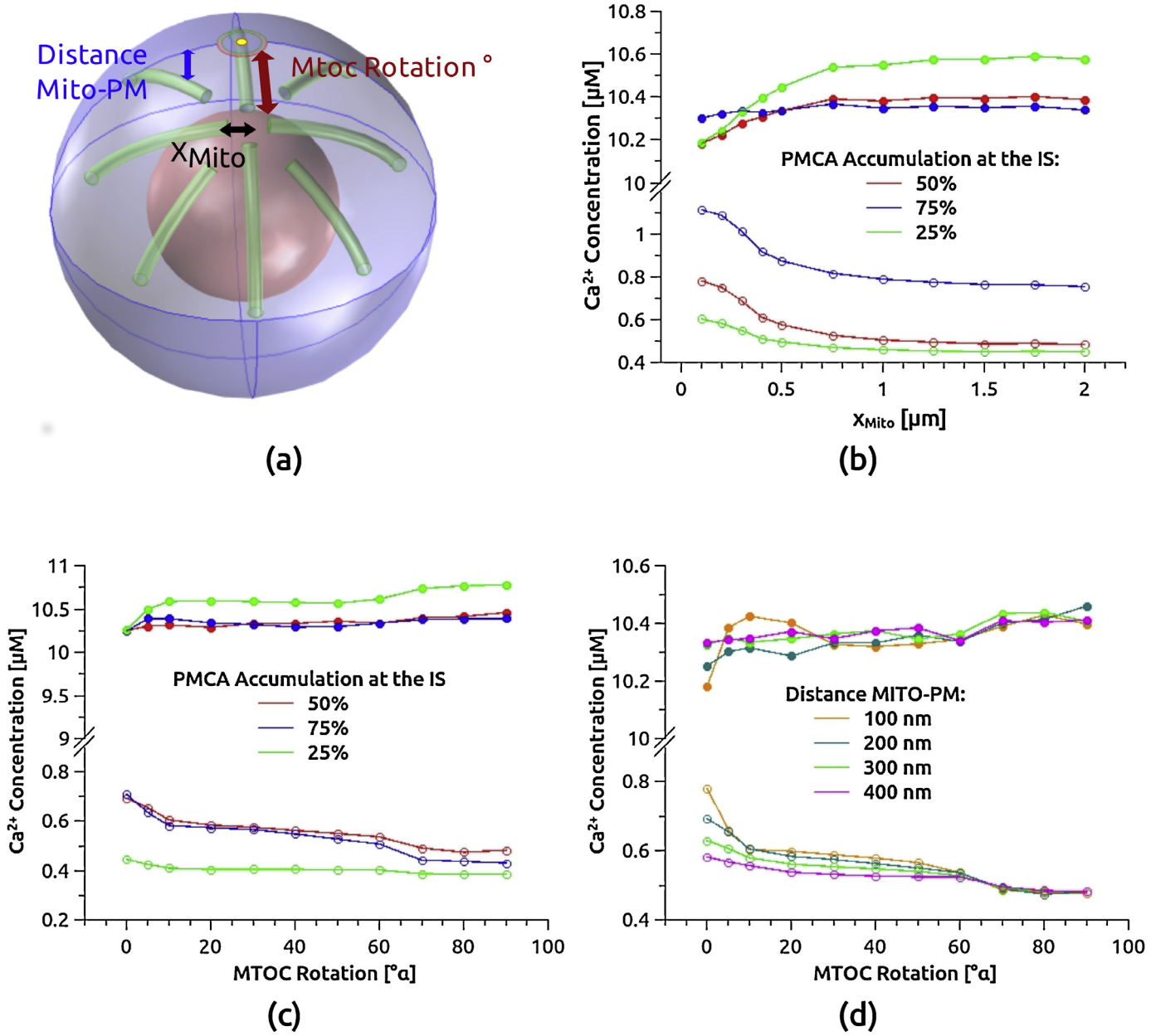

Fig. 4. Ca^{2+} concentrations depend on mitochondria rotation angle – model prediction for blocked SERCAS. **(a)** Sketch of the cell boundary (outer sphere), cell nucleus (inner sphere), IS (red circle), CRAC channels (yellow) and mitochondria geometry (green) for the model with depleted ER and blocked SERCAs. **(b)** Stationary value of the global (bottom curves) and local (top curves) Ca^{2+} concentrations predicted by the model as a function of the distance, x_{mito}, of the tip of the mitochondria from the CRAC channels in the fully polarized state (rotation angle $\alpha = 0$). **(c)** Stationary value of the global (bottom curves) and local (top curves) Ca^{2+} concentrations predicted by the model as a function of the rotation angle α for different levels of PMCA accumulation at the IS. **(d)** The same as in (c) but for different distances between mitochondria and plasma membrane. (For interpretation of the references to color in this figure legend, the reader is referred to the web version of this article.)

are located in the center of the IS in agreement with previous studies [23,36], PMCA pumps are in-homogeneously distributed over the plasma membrane with a higher concentration at the IS and a lower concentration on the rest of the PM in agreement with previous data [23]. The effect of mitochondrial Ca^{2+} uniporter and Na/Ca exchanger is described by in- and out-flux densities on the mitochondrial membranes. Similarly, the effect of IP_3 receptors and SERCA pumps on the Ca^{2+} content of the ER is described by in- and out-flux densities on the ER boundary. The precise definition and flux dependencies on Ca^{2+} concentrations in the different compartments can be found in the Materials and Methods section.

First we consider the experimental situation described above, in which SERCAs are blocked by thapsigargin, ER is empty and therefore CRAC channels fully activated. We computed the stationary Ca^{2+} distribution for different rotation angles as predicted by our model and show the results in Fig. 4. Fig. 4b shows the result for the fully polarized mitochondrial spindle (rotation angle $\alpha = 0$) as a function of the distance x_{mito} between the tips of the mitochondria and the CRAC channels for different PMCA accumulation levels. As already observed before [33], the global Ca^{2+} concentration increases with decreasing distance x_{mito}, whereas the local Ca^{2+} decreases. The variation becomes more pronounced the larger the PMCA accumulation level at the IS is. Next we fixed x_{mito} and varied the rotation angle α. As shown in Fig. 4c the global Ca^{2+} concentration increases with decreasing rotation angle of the mitochondrial spindle, most sharply for the smallest angle. The increase is again the more pronounced the higher the percentage of PMCA pumps accumulated at the IS. Simultaneously the local Ca^{2+} concentration

Please cite this article in press as: I. Maccari, et al., Cytoskeleton rotation relocates mitochondria to the immunological synapse and increases calcium signals, Cell Calcium (2016), http://dx.doi.org/10.1016/j.ceca.2016.06.007

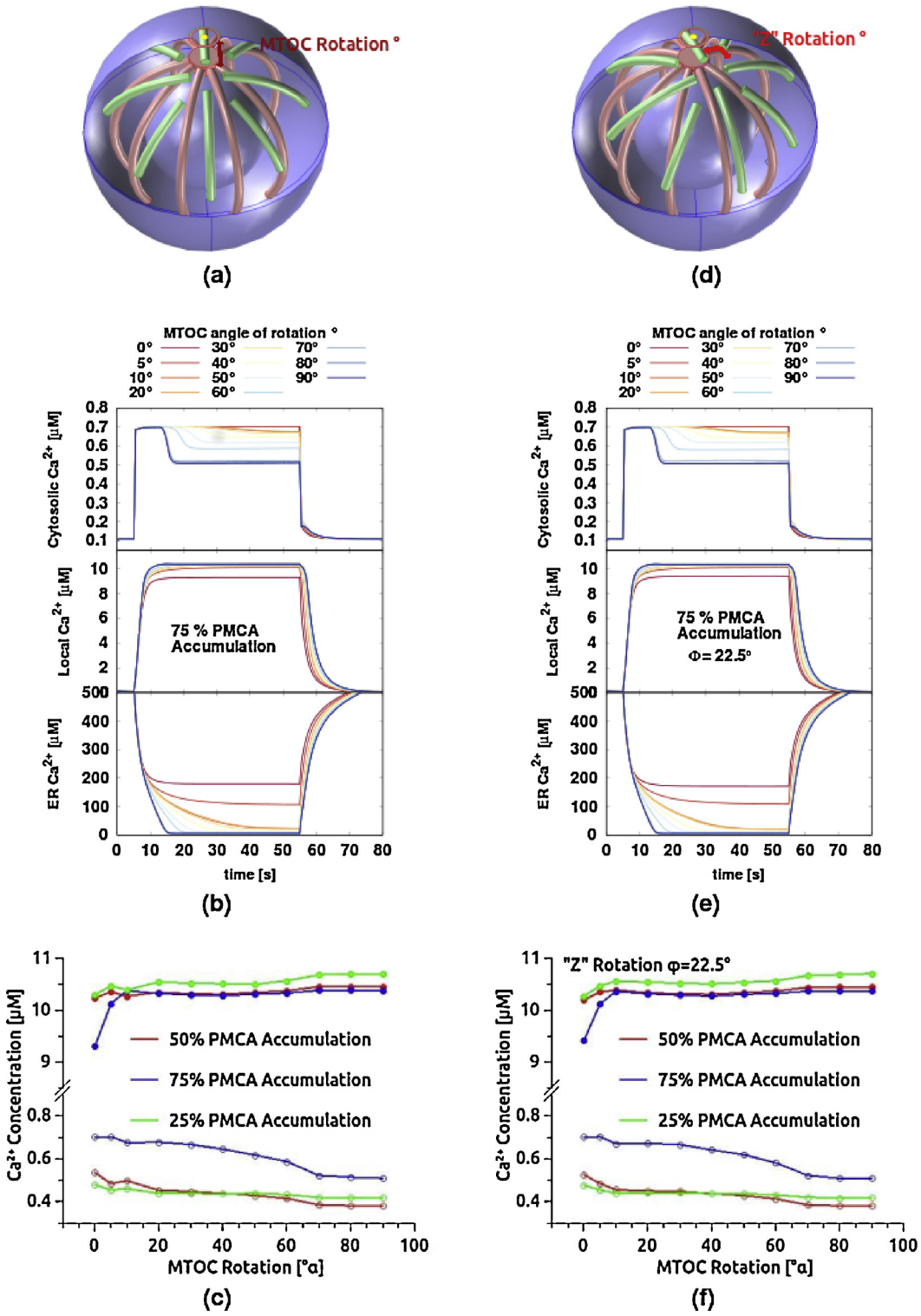

Fig. 5. Ca^{2+} concentrations depend on mitochondria rotation angle – model prediction with working SERCAs and spindle ER geometry. **(a)** Sketch of the mitochondria (green) and a spindle ER geometry (red). **(b)** Time course of Ca^{2+} concentrations in the cytosol (top), at the IS (middle), and in the ER (bottom) for the geometry in a. CRAC channels are activated at t = 10 s and deactivated at t = 60 s **(c)** Plateau value (at t = 40s) of the cytosol (global) and IS (local) Ca^{2+} concentrations as a function of the rotation angle of the mitochondrial network for different ratio of PMCA accumulation at the IS. **(d)** Same as in (a) but with mitochondria spindle rotatetd by 22.5 °. **(e)** Same as in (b) but for geometry d. **(f)** Same as in (c) but for geometry (d). (For interpretation of the references to color in this figure legend, the reader is referred to the web version of this article.)

at the IS decreases with decreasing rotation angle of the mitochondrial spindle, again more strongly with higher PMCA accumulation at the IS. The strength of the effect also depends on the distance between the mitochondria and the plasma membrane: the larger the distance the weaker the concentration changes with rotation angle (see Fig. 4d).

The physical reason for Ca^{2+} concentration changes is the following: with decreasing rotation angle the center of the mitochondrial spindle comes closer to the IS. The density of mito-

Please cite this article in press as: I. Maccari, et al., Cytoskeleton rotation relocates mitochondria to the immunological synapse and increases calcium signals, Cell Calcium (2016), http://dx.doi.org/10.1016/j.ceca.2016.06.007

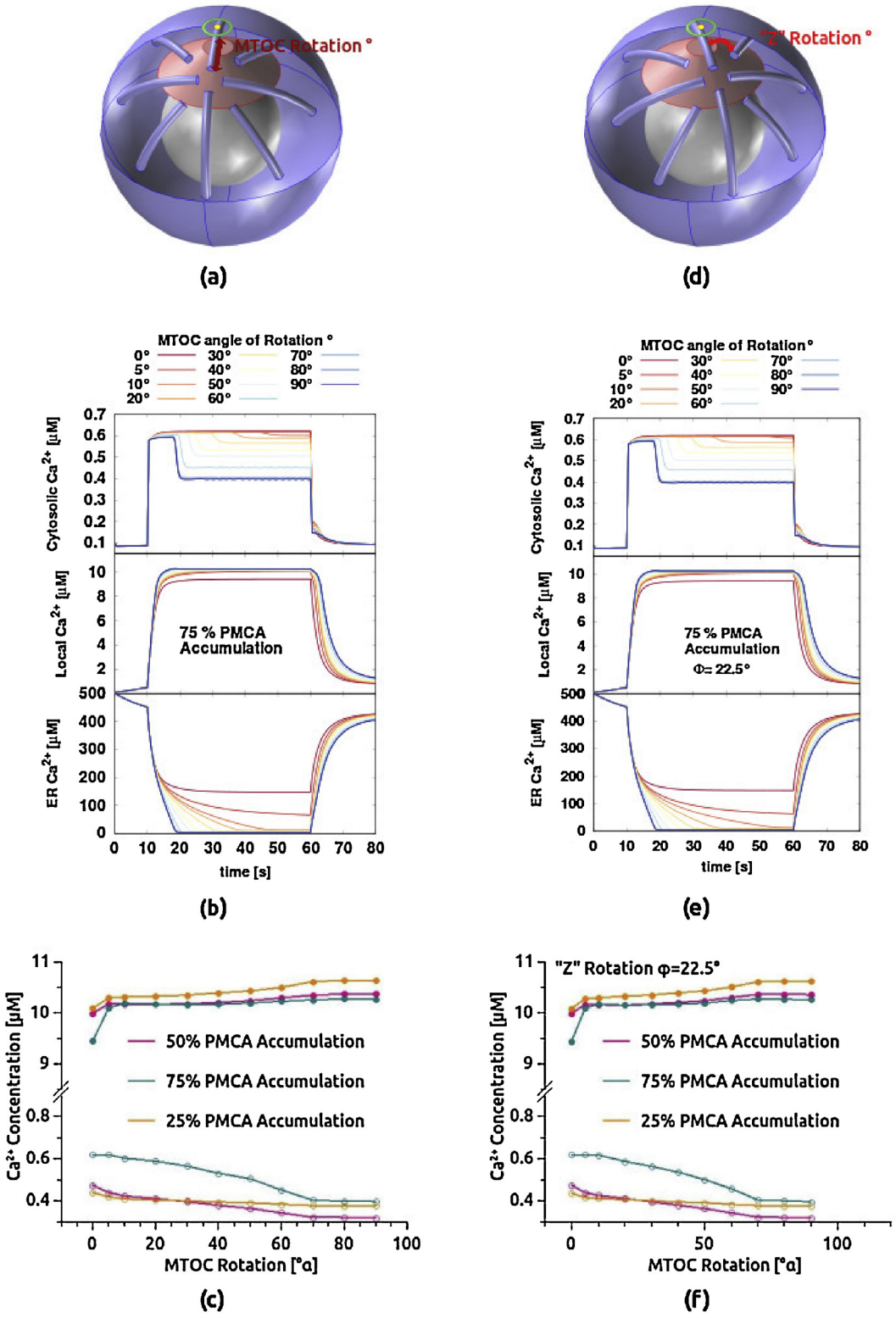

Fig. 6. Ca^{2+} concentrations depend on mitochondria rotation angle – model prediction with working SERCAs and truncated cone ER geometry. **(a)** Sketch of the mitochondria (green) and a truncated cone ER geometry (red). **(b)** Time course of Ca^{2+} concentrations in the cytosol (top), at the IS (middle), and in the ER (bottom) for the geometry in a. CRAC channels are activated at t = 10 s and deactivated at t = 60 s **(c)** Plateau value (at t = 40 s) of the cytsol (global) and IS (local) Ca^{2+} concentrations as a function of the rotation angle of the mitochondrial network for different ration of PMCA accumulation at the IS. **(d)** Same as in (a) but with mitochondria spindle rotatetd by 22.5 °. **(e)** Same as in (b) but for geometry d. **(f)** Same as in (c) but for geometry d. (For interpretation of the references to color in this figure legend, the reader is referred to the web version of this article.)

Please cite this article in press as: I. Maccari, et al., Cytoskeleton rotation relocates mitochondria to the immunological synapse and increases calcium signals, Cell Calcium (2016), http://dx.doi.org/10.1016/j.ceca.2016.06.007

chondria is highest at the center of the spindle, which means that more Ca^{2+} is transported into the mitochondrial compartment when the spindle center, supposed to be co-localized with the MTOC, comes close to the center of the IS, where the CRAC channels are located. Here the mitochondria take up the Ca^{2+} entering the microdomain underneath the IS, thereby decreasing the local Ca^{2+} concentration, and distribute it via internal diffusion along the mitochondrial lumen deeper into the cell, and release it into the cytosol, where less PMCAs are located, thereby increasing the global Ca^{2+} concentration.

2.5. Mathematical modeling predicts global Ca^{2+} increase during polarization under physiological conditions

Next we ask whether the Ca^{2+} concentration changes and the identified underlying mechanism observed with blocked SERCAs is relevant under more physiologically relevant conditions without administration of thapsigargin. We added a third compartment to our model, the ER, for which we assumed two different geometries: one also spindle-like, the other a truncated coned, both with fixed positions underneath the IS, see Figs. 5a and 6a, and in Figs. 5d and 6d for mitochondria rotated by 22.5° around the z-axis. The location of the ER is attributed to the fact that a part of the ER plasma membrane should be close to the IS to ensure CRAC channel formation through STIM-ORAI interaction. Ca^{2+} in- and out-flux is again modeled by a homogeneous density of SERCAs and IP_3-receptors, respectively, over the ER surface. The CRAC channel capacity now depends on the ER calcium concentration as originally proposed by Putney [37], a concept that has been widely recognized in many cell types. The precise definition and flux dependencies on Ca^{2+} concentrations in the different compartments are found in the Materials and Methods section.

Under physiological conditions an external stimulus, for instance provided by ligand binding to a G protein coupled or tyrosine kinase receptor, will increase the cytosolic IP_3 concentration. IP_3 binds to IP_3 receptors on the ER membrane allowing Ca^{2+} outflux from the ER through the channel domain of the receptors. The negative feedback that increased cytosolic Ca^{2+} has on the IP_3 receptor channel capacity, potentially leading to Ca^{2+} oscillations [38], is also considered in our simulations via the Ca^{2+} concentration dependent flux J_{IP3}. Once Ca^{2+} is released from the ER, CRAC channels open and SERCAs start to replenish the ER with Ca^{2+}. Consequently the dynamics of Ca^{2+} concentration is more complex than in the case of blocked SERCAs.

We assume the presence of an external stimulus between time t = 10 s and t = 40 s and computed the time course of the Ca^{2+} concentration in the different compartments for different rotation angles as predicted by our model. The results are shown in Fig. 5b for the spindle-like ER and in Fig. 5e with mitochondria rotated by 22.5° around the z-axis. The cytosolic Ca^{2+} concentration increases rapidly as soon as the stimulus starts and then decreases again slightly as usually reported in T cells, depending on how close the mitochondrial spindle center is to the IS, until a plateau value is reached. The plateau value is higher the smaller the rotation angle, i.e. the closer the mitochondrial spindle center is to the IS, and the local Ca^{2+} concentration at the IS is lower for smaller rotation angles, both in accordance with what is observed with blocked SERCAs (Fig. 1a and b, and [23]) but also consistent with the experiments with unblocked SERCAs [23]. The absolute value of the local Ca^{2+} concentration is around 10 μmol, which is in good agreement with recent simulations at the ER-plasma membrane junction with clustered Orai1 channels [39]. It is an average over a pre-defiend region around the CRAC channel and because of the steep Ca^{2+} gradient there depends on the size of this region. Therefore it cannot be compared directly with the experimental measurement depicted in Fig. 1.

The initial overshoot in the global Ca^{2+} concentration is due to the additional Ca^{2+} released by the ER and softens for smaller rotation angles. CRAC channels inactivation and PMCA modulation may also contribute to the overshoot. The ER Ca^{2+} concentration reaches a plateau, which is close to zero for large rotation angles but significantly larger than zero for small rotation angles. Once the stimulus is removed (at t = 40 s) all Ca^{2+} concentrations go back to baseline.

The mechanism of Ca^{2+} redistribution within the cell interior by the mitochondria and preventing Ca^{2+} entering the cell through the CRAC channels from being transported out again through the PMCA pumps is working in the physiological situation considered here, too. In addition the increased cytosolic Ca^{2+} concentration for small rotation angles lets the SERCAs replenish the ER at least partially, having an only minor effect on CRAC channel capacity.

In Fig. 5c and f we show the plateau values of global and local Ca^{2+} concentrations during stimulation for different PMCA pump accumulations at the IS as a function of the rotation angle. We observe qualitatively the same behavior as in the case of blocked SERCAs, i.e. a strong increase of the global Ca^{2+} concentration and decrease of the local one for a high accumulation of PMCAs at the IS.

Fig. 6 shows the results for the truncated cone ER geometry: Fig. 6a is a sketch of the compartment geometry, Fig. 6d with mitochondria rotated by 22.5° around the z-axis. The time course of the Ca^{2+} concentrations in the different compartments, shown in Fig. 6b and e, are similar to the spindle-like ER geometry (Fig. 5b and e), also the plateau values of the global and local Ca^{2+} concentrations show similar rotation angle dependencies. These results indicate that the reported effects are independent of the details of the ER geometry.

2.6. Calcium concentration is further increased by mitochondrial movement along microtubules towards the IS

In the work by Morlino et al. [22], it was observed that after MTOC relocation to the IS mitochondria move actively by Miro-1 modulated motors along microtubules towards the IS and increase. The effect of such an additional movement with fully polarized microtubules on the global and local Ca^{2+} concentration as predicted by our model can be seen from Fig. 4b: decreasing the distance, x_{mito}, between the tips of the mitochondria and the CRAC channels increases the global Ca^{2+} concentration and decreases the local one, depending on the degree of PMCA accumulation at the IS.

3. Discussion

Following T cell activation, mitochondria localize to the IS [21–24] and control local and global Ca^{2+} concentrations in T cells [23,32,33]. The MTOC as a key guiding organelle moves to the IS within several minutes of IS formation [13,16]. We present experimental evidence that during polarization of T-cells following target cell contact, the microtubule network rotates towards the IS and drags mitochondria with it. Based on the observed geometric paths of mitochondria during polarization we have developed a full three-dimensional (3D) compartment model for the Ca^{2+} dynamics in T-cells, which includes specific geometries and spatial arrangements of mitochondria, ER, and immunological synapse as well as localization aspects of Orai channels and PMCA at the IS. A potential regulation of PMCA by STIM1, as reported by Ritchie et al. [40], was not included in the model, however the pump rates are in accordance with values reported in the literature [41] and should thus reflect reasonable Ca^{2+} pump rates in T cells.

The model predicts an increase of global Ca^{2+} and a decrease in local Ca^{2+} concentration in case the mitochondrial structure is rotated towards the IS and a fraction of PMCA pumps accumu-

Please cite this article in press as: I. Maccari, et al., Cytoskeleton rotation relocates mitochondria to the immunological synapse and increases calcium signals, Cell Calcium (2016), http://dx.doi.org/10.1016/j.ceca.2016.06.007

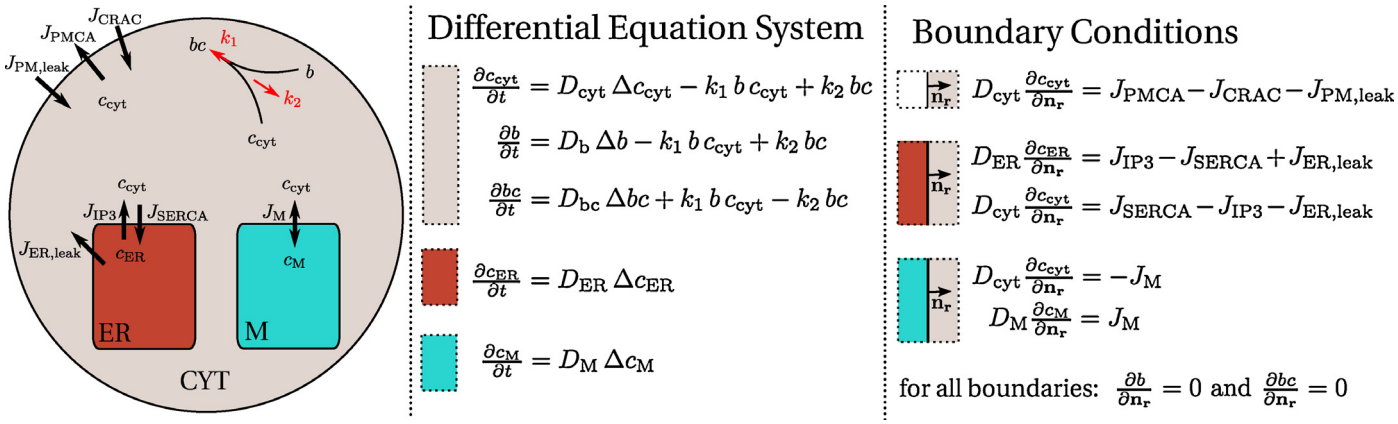

Fig. 7. Sketch of the mathematical model for the intracellular Ca^{2+} dynamics. For the figure description see Materials and Methods section.

lates at the IS, in agreement with experimental observations in thapsigargin-treated cells and in cells without thapsigargin present [23]. Once the cytoskeleton is fully polarized the mitochondria can still move further towards the IS along the microtubules, which the model predicts to increase global Ca^{2+} concentration even further and decrease local Ca^{2+} more.

The physical mechanism underlying the increase of the global Ca^{2+} concentration is, according to our model, the following: with decreasing rotation angles the center of the mitochondrial spindle comes closer to the IS. The density of mitochondria is highest at the center of the spindle, which means that more Ca^{2+} is transported into the mitochondrial compartment when the spindle center, supposed to be co-localized with the MTOC, comes close to the center of the IS, where the CRAC channels are located. Here the mitochondria take up the Ca^{2+} entering the microdomain underneath the IS, thereby decreasing the local Ca^{2+} concentration, and distribute it via internal diffusion along the mitochondrial lumen deeper into the cell, and release it into the cytosol, where less PMCAs are located, thereby increasing the global Ca^{2+} concentration.

The full cell 3D model also includes localization and structural determinants of the ER. Since the model predicts that the effect also persists under more physiological conditions, i.e. when SERCAs are functional, we can conclude that the ER is not involved in the control of local and global Ca^{2+} concentrations following T cell activation through the IS. This is also in agreement with experimental evidence [23]. Of course ER-bound STIM 1 or 2 are required to activate Orai channels but once they are activated, mitochondria take over to control the Ca^{2+} signal in T cells. They not only determine local and global Ca^{2+} but they redirect much of the Ca^{2+} away from the SERCAs into the cell center by the same mechanism as they redirect Ca^{2+} away from the PMCA pumps accumulated at the IS. Together with Orai channels, PMCA are also enriched at the IS whereas SERCA is not [23]. It is thus not surprising that in the absence of mitochondria at the IS (e.g. 2 μm away, compare Fig. 4b), the ER does not refill significantly because PMCA export the Ca^{2+}. In this case, Ca^{2+} cycles across the plasma membrane rather than fulfilling its cytosolic functions.

It was shown previously that CRAC channels partially inactivate if mitochondria are not able to accumulate Ca^{2+} [42], however these experiments were carried out under conditions with no IS formation and thus no enrichment of PMCA at certain plasma membrane sites. In case of IS formation the model clearly predicts that a change in CRAC activity is not required to explain the mitochondrial control of local and global Ca^{2+}, only PMCA enrichment at the IS is necessary. Thus in case of IS formation the model reveals a clear hierarchy for the incoming Ca^{2+}. If present at the IS, mitochondria take up the vast majority of Ca^{2+} incoming through CRAC channels, if not present, PMCA export Ca^{2+} incoming through CRAC channels, and if neither mitochondria are present nor PMCA are enriched at the IS, SERCAs and the ER take up Ca^{2+}, which finally inactivates Orai channels. In conclusion the experimentally described mitochondria, ER, Orai, PMCA and SERCA localization at the IS is well suited to guide Ca^{2+} entering the cell at the IS deeper into the cytosol and to control local Ca^{2+} at the IS. CRAC activity at the IS is not decreased as long as either mitochondria or PMCA or both are enriched at the IS preventing refilling of the ER.

4. Materials and Methods

4.1. 3-dimensional (3D) full cell Ca^{2+} model

Our model for the calcium homoeostasis in T-cells consists of several compartments with specific geometry as defined below. The three-dimensional geometry together with explicit incorporation of Ca^{2+} diffusion discriminates our model from other mathematical approaches based on spatially averaged Ca^{2+} concentrations [43]. Ca^{2+} can diffuse within the compartments and exchange Ca^{2+} via channels and pumps: the cell body or cytosol, the mitochondria, and the ER, as sketched in Figs. 4a, 5a, d, and 6a, d. The cell body represents an ideal spherical T-cell with radius $r_{cell} = 4\,\mu m$, and a spherical nucleus with radius $r_{nuc} = r_{cell}/2$. Mitochondrial filaments are assumed to have a rod-like shape with a length of 3.5 μm and a diameter of $d_M = 300$ nm, of which 4–10 are arranged in a spindle like geometry as indicated in Fig. 4a. Mitochondrial filaments can take up and release Ca^{2+} over their whole surface, described by a Ca^{2+} current J_M to be defined below. Inside mitochondria Ca^{2+} diffuses with a diffusion constant D_M.

At the IS, we assume an accumulation of CRAC channels into a cluster of radius $r_{CRAC} = 0.1\,\mu m$. At a distance of 0.3 μm to this CRAC cluster, a spherical segment of 100 nm width represents an agglomerate of PMCA pumps. In our Base Case scenario this spherical segment contains 50% of all pumps, whereas the other 50% are homogeneously distributed over the whole cell PM (according to fluorescence it is more like 70% at the IS, compare [23]). Inside the cytosol, Ca^{2+} is buffered by a mobile Ca^{2+} buffer b that freely diffuses with constant D_b. The total amount of buffer $[b]_T = [b] + [bc]$ is initially uniform in the cytosol for which we assumed that the binding of Ca^{2+} does not change the diffusion properties of the buffer. We use various geometries for the ER to be defined below. The naturally very thin ER network is modeled as a massive domain and therefore we assume that it is invisible for the cytosolic Ca^{2+}, which means that in the model cytosolic Ca^{2+} freely diffuses through the ER domain.

Please cite this article in press as: I. Maccari, et al., Cytoskeleton rotation relocates mitochondria to the immunological synapse and increases calcium signals, Cell Calcium (2016), http://dx.doi.org/10.1016/j.ceca.2016.06.007

The spatio-temporal evolution of Ca^{2+} (and buffer) concentrations in the different compartments follows reaction-diffusion equations with sources and sinks as sketched in Fig. 7 and is defined in the following:

$$\frac{\partial c_{cyt}}{\partial t} = D_{cyt}\Delta c_{cyt} - k_1 c_{cyt} b + k_2 bc$$

$$\frac{\partial b}{\partial t} = D_b \Delta b - k_1 c_{cyt} b + k_2 bc$$

$$\frac{\partial bc}{\partial t} = D_{bc}\Delta bc + k_1 c_{cyt} b - k_2 bc$$

$$\frac{\partial c_M}{\partial t} = D_M \Delta c_M$$

$$\frac{\partial c_{ER}}{\partial t} = D_{ER}\Delta c_{ER}$$

The Ca^{2+} currents through the plasma membrane, J_{PM}, and the compartment membranes of the ER, J_{ER}, and the mitochondria, J_M, are implemented as flux/boundary conditions on the 2d surfaces separating the corresponding compartments and defined as follows.

The Ca^{2+} exchange across the plasma membrane, J_{PM}, contains two contributions: $J_{PM} = J_{CRAC} - J_{PMCA}$, where J_{CRAC} represents the influx through the CRAC channels and J_{PMCA} represents the export of Ca^{2+} pumped out of the cytosol via the PMCA pumps. J_{CRAC} is only defined on the CRAC cluster surface. The cluster influx is coupled to the Ca^{2+} concentration within the ER (c_{ER}) and at the average calcium concentration ($c_{cyt}^{(micro)}$) in the micro-domain around the cluster in the following way:

$$J_{CRAC} = k_{CRAC} f_1(c_{ER}) g_{c_{1/2},\Delta c}\left(c_{cyt}^{(micro)}\right)$$

where $f_1(x)$ and $g_{c_{1/2},\Delta c}(x)$ are both smooth sigmoid-shaped functions modeling the CRAC activation by emptied ER and CRAC inhibition by an enhanced Ca^{2+} concentration in the microdomain, respectively. We assume $f_1(x) = 0$ for a full store $x > 500\,\mu M$, $f_1(x) = 1/2$ for $x = 250\,\mu M$ and $f_1(x) = 1$ for an empty store ($x = 0\,\mu M$). The function $g_{c_{1/2},\Delta c}(x)$ varies smoothly from $g_{c_{1/2},\Delta c}(x) = 1$ for $x \leq c_{1/2} - \Delta_c$ to $g_{c_{1/2},\Delta c}(x) = 0$ for $x \geq c_{1/2} + \Delta_c$.

The plasma membrane Ca^{2+} pump currents at the IS and the plasma membrane is given by

$$J_{PMCA,PM} = k_{PMCA,IS}\frac{c_{cyt}^2}{k_p^2 + c_{cyt}^2} \quad \text{and} \quad J_{PMCA} = k_{PMCA,PM}\frac{c_{cyt}^2}{k_p^2 + c_{cyt}^2}$$

where the maximum pump rates $k_{PMCA,IS}$ and $k_{PMCA,PM}$ depend on the PMCA accumulation at the IS and on the area ratio of IS and the remaining PM.

The Ca^{2+} exchange across the ER surface, $J_{ER} = J_{IP3} - J_{SERCA}$, comprises Ca^{2+} release from the ER through the IP_3 receptor channels into the cytosol, J_{IP3}, and the Ca^{2+} pumped back through the SERCAs from the cytosol into the ER, J_{SERCA}. The first contribution to the current J_{ER} is:

$$J_{IP3} = k_{IP3}\theta(t_{IP3} - t) g_{c_{1/2}^{IP3},\Delta_c^{IP3}}(c_{cyt}) f_2(c_{ER})$$

We assume fully activated IP_3 receptor channels during the specified time period t_{IP3}. For time $t > t_{IP3}$ the flux J_{IP3} is equal to zero; otherwise its release rate depends on c_{cyt} [38] and on c_{ER} through the two sigmoidal-shaped functions $g_{c_{1/2}^{IP3},\Delta_c^{IP3}}(x)$ and $f_2(x)$: the first one models the IP_3 channels open probability (which depends on c_{cyt}), the second models the channels inhibition due to low values of c_{ER}. In particular we set $f_2(x) = 1$ for $x \geq 200\mu M$, $f_2(x) = 1/2$ for $x = 100\mu M$ and $f_2(x) = 0$ for $x = 0\mu M$.

The Ca^{2+} back-flux into the ER caused by the SERCA pumps is assumed to be given by

$$J_{SERCA} = k_{SERCA}\frac{c_{cyt}^2}{c_{cyt}^2 + k_{ER}^2}$$

where k_{ER}, as in the previous cases, represents the value of the cytosolic concentration at which the pumps work at the half of their maximal efficiency k_{SERCA}.

The Ca^{2+} current across the mitochondria surface comprises influx through the mitochondrial Ca^{2+} uniporter (MCU) and export by the Na/Ca exchanger. Physiologically, Ca^{2+} uptake through the MCU would depolarise the mitochondria, reducing further influx. We model this effect in a 2nd order Michaelis-Menten form of the inward flux:

$$J_M = k_{inward}\cdot\frac{{c_{cyt}}^2}{c_{cyt}^2 + {k_{m1}}^2} - k_{out}\cdot\frac{c_M}{c_M + k_{m2}}$$

To simulate experiments in which the SERCA pumps are blocked by thapsigargin, leading to an emptied ER and fully activated CRAC channels we omit the boundary conditions involving c_{ER} and set $J_{CRAC} = k_{CRAC} g_{c_{1/2},\Delta c}\left(c_{cyt}^{(micro)}\right)$.

To solve our reaction–diffusion equations, we use the package 'transport of diluted species' of the finite elements method software 'Comsol' (http://www.comsol.com/).

4.1.1. Parameters

For the Ca^{2+} diffusion constant in the cytosol we use the estimate of $D_{cyt} = 200\,\mu m^2/s$ [44], and set the Ca^{2+} diffusion constant in mitochondria to $D_M = D_{cyt}$ and in the ER to a smaller value $D_{ER} = D_{cyt}/10$. Also the diffusion of mobile Ca^{2+} buffers is usually smaller, with $D_b = D_{bc} = D_{cyt}/20$ [45]. The reaction rates for Ca^{2+} binding and unbinding k_1 and k_2 and the buffer resting concentration are in good agreement with commonly used modeling parameters [46].

The CRAC channel influx parameter was set to $k_{CRAC} = 5{\cdot}10^{-5}\,mol/m^2\,s$. Since CRAC channels are modeled as an area of size $A_{CRAC} = 3.1{\cdot}10^{-14}\,m^2$, the total channel capacity is $1.55{\cdot}10^{-17}\,mol/s$, which is equivalent to $9.3{\cdot}10^5$ particles/s, corresponding to a CRAC cluster of 93 fully activated CRAC channels.

For the PMCA pumps we use globally (i.e. no PMCAs at the IS) $k_{PMCA,gloabal} = 8{\cdot}10^{-9}\,mol/m^2\,s$. With a plasma membrane area of $A_{PM} = 2{\cdot}10^{-10}\,m^2$ this corresponds to $1.6{\cdot}10^{-18}\,mol/s$ or 26,000 particles/s. A single PMCA pumps about 10 particles/s, which means that we assume 2600 pumps in total on the PM or 13 pumps/μm in accordance with values reported in the literature [41]. When in our base case scenario 50% of the PMCA pumps are assumed to be located in a ring of width $0.1/\mu m$ and radius $0.3/\mu m$ amount the center of the IS this implies $k_{PMCA,IS} = 3{\cdot}10^{-6}\,mol/m^2\,s$ and $k_{PMCA,PM} = 4{\cdot}10^{-9}\,mol/m^2\,s$.

As discussed in Ref. [33], the parameter of the Ca^{2+} flux across mitochondria boundaries are chosen such that total maximum currents through PMCA pumps and across mitochondria boundaries are approximately equal $I_{PMCA}^{max}/I_M^{max} \approx 1$.

The SERCA flux parameter is set to $k_{SERCA} = 3.5{\cdot}10^{-8}\,m/s$. Since the ER area is $A_{ER} = 6{\cdot}10^{-9}\,m^2$ the maximum SERCA pump capacity is $1.3{\cdot}10^6$ particles/s. A single SERCA pumps 5–10 particles/s so that we have ca. 500,000 pumps, which is in agreement with the values used in Refs. [43,47,48]. For the IP_3 channels we assume a maximum flux rate of $k_{IP3} = 10{\cdot}k_{SERCA}$.

All parameters for the base case scenario together with the initial conditions for Ca^{2+} concentrations in the different compartments are summarized in Table 1. For the truncated cone geometry

Please cite this article in press as: I. Maccari, et al., Cytoskeleton rotation relocates mitochondria to the immunological synapse and increases calcium signals, Cell Calcium (2016), http://dx.doi.org/10.1016/j.ceca.2016.06.007

Table 1
Parameters and initial values used for the Base Case scenario in our 3D cell model.

Parameter	Value (unit)	Parameter	Value (unit)
D_{cyt}	200 ($\mu m^2\ s^{-1}$)	k_{CRAC}	$5{\cdot}10^{-5}$ (mol/m^2 s)
D_M	200 ($\mu m^2\ s^{-1}$)	$k_{PMCA,IS}$	$3{\cdot}10^{-6}$ (mol/m^2 s)
D_b	10 ($\mu m^2\ s^{-1}$)	$k_{PMCA,PM}$	$4{\cdot}10^{-9}$ (mol/m^2 s)
D_{bc}	10 ($\mu m^2\ s^{-1}$)	k_{SERCA}	$3.5{\cdot}10^{-8}$ (m/s)
D_{ER}	20 ($\mu m^2\ s^{-1}$)	k_{IP3}	$3.5{\cdot}10^{-7}$ (m/s)
$c_{cyt}(t=0)$	100 (nM)	k_{inward}	$9{\cdot}10^{-6}$ (mol/m^2 s)
$c_M(t=0)$	100 (nM)	k_{out}	$8{\cdot}10^{-6}$ (mol/m^2 s)
$c_{ER}(t=0)$	500 (μM)	k_p	300 (nM)
$c_b(t=0)$	10 (μM)	k_{m1}	600 (nM)
$c_{bc}(t=0)$	500 (nM)	k_{m2}	15 (μM)
A_{CRAC}	$3.1{\cdot}10^{-14}$ (m^2)	k_{ER}	300 (nM)
A_{PM}	$2{\cdot}10^{-10}$ (m^2)	$c_{1/2}$	15 (μM)
A_M	$2.44{\cdot}10^{-11}$ (m^2)	Δ_c	1 (μM)
A_{ER}	$5.9{\cdot}10^{-11}$ (m^2)	$c_{1/2}^{IP3}$	600 (nM)
J_{PMleak}	$4.5{\cdot}10^{-10}$ (mol/m^2 s)	Δ_c^{IP3}	200 (nM)
J_{ERleak}	$3.5{\cdot}10^{-9}$ (mol/m^2 s)	k_1	100 (m^3/mol s)
k_2	0.3 s^{-1}		.

of the ER we have adapted the parameters for k_{SERCA}, k_{IP3}, and $J_{ER,leak}$ to accommodate for the smaller ER surface A_{ER} in order to maintain the maximum number of Ca^{2+} particles per second into the ER: $A_{ER} = 2.7{\cdot}10^{-9}$ m^2, $k_{SERCA} = 7.6{\cdot}10^{-8}$ m/s, $k_{IP3} = 7.6{\cdot}10^{-7}$ m/s, and $J_{ER,leak} = 7.6{\cdot}10^{-9}$ mol/m^2 s.

4.2. Cell culture

Human Jurkat E6.1 cells were grown in RPMI 1640 medium supplemented with 10% FCS and penicillin-streptomycin and maintained in log-phase. Peripheral blood mononuclear cells (PBMC) were obtained from healthy donors as previously described [49]. CTL stimulated with CD3/CD28 beads were prepared as described before [12]. Raji cells were cultured in RPMI-1640 medium (ThermoFisher Scientific) supplemented with 10% FCS.

4.3. Evanescent-wave imaging

TIRFM experiments were carried out exactly as the ones shown in Fig. 4C, D of our publication by Quintana et al. [23] and are described there. The only difference is that here, the local and global Ca^{2+} concentrations were measured in two different sets of cells and not in the same cells.

The following solutions were used: 155 NaCl, 4.5 KCl, 1 $CaCl_2$, 2 $MgCl_2$, 10 D-glucose, and 5 Hepes (pH 7.4 with NaOH). $CaCl_2$ was replaced by 1 mM EGTA for the 0 Ca^{2+} or increased for the 20 mM Ca^{2+} solution. Chemicals not specifically mentioned were from Sigma (highest grade). Fluo-5F (stock 1 mM in DMSO) was from Molecular Probes and anti-human CD3 monoclonal antibodies were from Biozol.

4.4. Plasmids and reagents

All chemicals not specifically mentioned were from Sigma (highest grade). EMTB-3 × GFP and DsRed2-Mito-7 were purchased from AddGene. MitoTracker Deep Red FM was purchased from Life Technologies.

4.5. Time-lapse imaging

CTL were transfected with EMTB-3 × GFP alone or with DsRed2-Mito-7. Mitochondria were labeled with MitoTracker Deep Red FM or DsRed2-Mito-7 as indicated in the figure legend. Raji cells were pulsed with SEA (0.1 μg/ml)/SEB (0.1 μg/ml) at 37 °C for 30 min before conjugation with CTL. CTL were settled on poly-L-ornithine coated coverslips, and then target cells were given into the medium. The translocation of microtubule network (EMTB-3 × GFP, green channel) and mitochondria (red channel or far-red channel) in CTL was visualized at 37 °C using a confocal (Zeiss) equipped with a 63 × objective (NA 1.4). The step-size of z-stacks is 1 μm. The time interval between each stack is 19.02–21.17 s. For spinning disk confocal microscope CTL were settled on CD3/CD28 antibody-coated coverslips, and the images were acquired at room temperature every 4.66 s with a z-stack step-size of 0.79 μm.

4.6. Extraction of rotation angles from tracking data

From time-lapse imaging obtained with the spinning disk microscope with a time interval of 4.66 s we extracted for each z-stack between 0 s (start of polarization) and 186.4 s (end of polarization) the three-dimensional position coordinates of MTOC, IS, and individual mitochondria (precisely: the center of the light spots indicating their position). The position of the cell center was estimated via a weighted average of the centers of the cross-section of individual planes of the z-stack, where the areas of the cross-sections were used as weight. The cell center was determined for each frame individually.

Since the cell was not stable during the measurement the movement of the cell as a whole had to be subtracted. The cell has three translational and two rotational degrees of freedom. For every z-stack, values of coordinates of the center were subtracted from values of coordinates of mitochondria, MTOC and IS.

Next the position data for all objects in a z-stack were brought into a standard coordinate system by two rotations: In the first one, IS rotates to z axis and MTOC and mitochondria rotate accordingly. In the second rotation, MTOC is moved to x-z plane. The coordinates of mitochondria are transformed by the same manner. IS is always on z axis and MTOC rotates just in x-z plane and the y-axis is the axis of rotation.

We defined the following vectors $\rightarrow MTOC = \rightarrow MT - \rightarrow CT$, $\rightarrow IS = \rightarrow is - \rightarrow CT$, and $\rightarrow mito_i = \rightarrow mt_i - \rightarrow CT_i$, where $\rightarrow MT$, $\rightarrow is$, $\rightarrow CT$ and $\rightarrow mito_i$ are the coordinates of the MTOC, IS, center of the cell and mitochondria, respectively. During the repositioning of the MTOC the angles between the vectors $\rightarrow MTOC$ and $\rightarrow IS$ and between the vectors $\rightarrow mito_i$ and $\rightarrow IS$ change continuously and is recorded between two time frames.

During the rotation of the MTOC in the x-z plane the angle between the vectors $\rightarrow MTOC$ and $\rightarrow IS$ decreases (c.f. the sketch in Fig. 3a) and if the rotation of the whole cytoskeleton drags the mitochondria with it the angles between $\rightarrow mito_i$ and $\rightarrow IS$ have to change according to a rotation around the y-axis. The change of angle between $\rightarrow mito_i$ and $\rightarrow IS$ depends on initial position of mitochondria, or, more concretely, on half-space (left or right) where it is located (c.f. Fig. 3a). In the "right half-space" the angles between $\rightarrow mito_i$ and $\rightarrow IS$ get smaller, as is visible in Fig. 3b. Conversely, the rotation leads to enlargements of angles in "left half-space". To prove repositioning of mitochondria with microtubules, angles before and after repositioning were measured and results were compared. If the hypothesis of a correlated repositioning of mitochondria and microtubules is true, the angles after repositioning should be smaller at the "right half-space" and lower at the "left half-space". The histograms in Fig. 3b and c indeed show the expected changes of angles during repositioning and demonstrate the rotation of mitochondria with the MTOC/microtubule part of the cytoskeleton.

Author contributions

M., M.P., K.S. and I.H., H.R. designed and performed all modelling parts. R.Z. performed and analyzed experiments relevant for Figs. 2

Please cite this article in press as: I. Maccari, et al., Cytoskeleton rotation relocates mitochondria to the immunological synapse and increases calcium signals, Cell Calcium (2016), http://dx.doi.org/10.1016/j.ceca.2016.06.007

and 3. A.Q. and M.P. performed and analyzed experiments shown in Fig. 1. I.M. and R.Z. are responsible for the layout of the figures. H.R. designed the study with contributions from B.Q. and M.H. The manuscript was written by H.R. and M.H. with B.Q. adding parts regarding the experimental data. All authors edited the manuscript and concurred with the submission.

Acknowledgements

Research carried out for this study with human material (leukocyte reduction system chambers from human blood donors) is authorized by the local ethic committee (declaration from 16.4.2015 (84/15; Prof. Dr. Rettig-Stürmer)). We thank Ute Becherer (Saarland University) for help with TIRF microscopy. We thank the Institute for Clinical Hemostaseology and Transfusion Medicine for providing donor blood; Carmen Hässig and Gertrud Schwär for excellent technical help. This project was funded by Sonderforschungsbereich CRC 1027 project A3 (to H.R.) and A2 (to B.Q. and M.H.).

References

[1] D. Pruyne, A. Legesse-Miller, L. Gao, Y. Dong, A. Bretscher, Mechanisms of polarized growth and organelle segregation in yeast, Annu. Rev. Cell Dev. Biol. 20 (2004) 559–591.
[2] P. van Bergeijk, C.C. Hoogenraad, L.C. Kapitein, Right time, right place: probing the functions of organelle positioning, Trends Cell Biol. 26 (2016) 121–134.
[3] N.B. Martin-Cofreces, F. Baixauli, F. Sanchez-Madrid, Immune synapse: conductor of orchestrated organelle movement, Trends Cell Biol. 24 (2014) 61–72.
[4] G.M. Griffiths, A. Tsun, J.C. Stinchcombe, The immunological synapse: a focal point for endocytosis and exocytosis, J. Cell Biol. 189 (2010) 399–406.
[5] A. Quintana, M. Hoth, Mitochondrial dynamics and their impact on T cell function, Cell Calcium 52 (2012) 57–63.
[6] K.L. Angus, G.M. Griffiths, Cell polarisation and the immunological synapse, Curr. Opin. Cell Biol. 25 (2013) 85–91.
[7] M.L. Dustin, E.O. Long, Cytotoxic immunological synapses, Immunol. Rev. 235 (2010) 24–34.
[8] J.S. Orange, Formation and function of the lytic NK-cell immunological synapse, Nat. Rev. Immunol. 8 (2008) 713–725.
[9] R. Wedlich-Soldner, S. Altschuler, L. Wu, R. Li, Spontaneous cell polarization through actomyosin-based delivery of the Cdc42 GTPase, Science 299 (2003) 1231–1235.
[10] D. Obino, F. Farina, O. Malbec, P.J. Saez, M. Maurin, J. Gaillard, F. Dingli, D. Loew, A. Gautreau, M.I. Yuseff, L. Blanchoin, M. Thery, A.M. Lennon-Dumenil, Actin nucleation at the centrosome controls lymphocyte polarity, Nat. Commun. 7 (2016) 10969.
[11] H.T. Hsu, J.S. Orange, Distinct integrin-dependent signals define requirements for lytic granule convergence and polarization in natural killer cells, Sci. Signal. 7 (2014) pe24.
[12] B. Qu, V. Pattu, C. Junker, E.C. Schwarz, S.S. Bhat, C. Kummerow, M. Marshall, U. Matti, F. Neumann, M. Pfreundschuh, U. Becherer, H. Rieger, J. Rettig, M. Hoth, Docking of lytic granules at the immunological synapse in human CTL requires Vti1b-dependent pairing with CD3 endosomes, J. Immunol. 186 (2011) 6894–6904.
[13] J.C. Stinchcombe, E. Majorovits, G. Bossi, S. Fuller, G.M. Griffiths, Centrosome polarization delivers secretory granules to the immunological synapse, Nature 443 (2006) 462–465.
[14] A.T. Ritter, Y. Asano, J.C. Stinchcombe, N.M. Dieckmann, B.C. Chen, C. Gawden-Bone, S. van Engelenburg, W. Legant, L. Gao, M.W. Davidson, E. Betzig, J. Lippincott-Schwartz, G.M. Griffiths, Actin depletion initiates events leading to granule secretion at the immunological synapse, Immunity 42 (2015) 864–876.
[15] G. de Saint Basile, G. Menasche, A. Fischer, Molecular mechanisms of biogenesis and exocytosis of cytotoxic granules, Nat. Rev. Immunol. 10 (2010) 568–579.
[16] J.C. Stinchcombe, L.O. Randzavola, K.L. Angus, J.M. Mantell, P. Verkade, G.M. Griffiths, Mother centriole distal appendages mediate centrosome docking at the immunological synapse and reveal mechanistic parallels with ciliogenesis, Curr. Biol. 25 (2015) 3239–3244.
[17] J.C. Stinchcombe, G.M. Griffiths, Communication, the centrosome and the immunological synapse, Philos. Trans. R. Soc. Lond. B Biol. Sci. 369 (2014).
[18] J. Yi, X. Wu, A.H. Chung, J.K. Chen, T.M. Kapoor, J.A. Hammer, Centrosome repositioning in T cells is biphasic and driven by microtubule end-on capture-shrinkage, J. Cell Biol. 202 (2013) 779–792.
[19] A. Kupfer, G. Dennert, Reorientation of the microtubule-organizing center and the Golgi apparatus in cloned cytotoxic lymphocytes triggered by binding to lysable target cells, J. Immunol. 133 (1984) 2762–2766.
[20] A. Kupfer, G. Dennert, S.J. Singer, Polarization of the Golgi apparatus and the microtubule-organizing center within cloned natural killer cells bound to their targets, Proc. Natl. Acad. Sci. U. S. A. 80 (1983) 7224–7228.
[21] F. Baixauli, N.B. Martin-Cofreces, G. Morlino, Y.R. Carrasco, C. Calabia-Linares, E. Veiga, J.M. Serrador, F. Sanchez-Madrid, The mitochondrial fission factor dynamin-related protein 1 modulates T-cell receptor signalling at the immune synapse, EMBO J. 30 (2011) 1238–1250.
[22] G. Morlino, O. Barreiro, F. Baixauli, J. Robles-Valero, J.M. Gonzalez-Granado, R. Villa-Bellosta, J. Cuenca, C.O. Sanchez-Sorzano, E. Veiga, N.B. Martin-Cofreces, F. Sanchez-Madrid, Miro-1 links mitochondria and microtubule Dynein motors to control lymphocyte migration and polarity, Mol. Cell. Biol. 34 (2014) 1412–1426.
[23] A. Quintana, M. Pasche, C. Junker, D. Al-Ansary, H. Rieger, C. Kummerow, L. Nunez, C. Villalobos, P. Meraner, U. Becherer, J. Rettig, B.A. Niemeyer, M. Hoth, Calcium microdomains at the immunological synapse: how ORAI channels, mitochondria and calcium pumps generate local calcium signals for efficient T-cell activation, EMBO J. 30 (2011) 3895–3912.
[24] A. Quintana, C. Schwindling, A.S. Wenning, U. Becherer, J. Rettig, E.C. Schwarz, M. Hoth, T cell activation requires mitochondrial translocation to the immunological synapse, Proc. Natl. Acad. Sci. U. S. A. 104 (2007) 14418–14423.
[25] C. Schwindling, A. Quintana, E. Krause, M. Hoth, Mitochondria positioning controls local calcium influx in T cells, J. Immunol. 184 (2010) 184–190.
[26] T.A. Lyubchenko, G.A. Wurth, A. Zweifach, Role of calcium influx in cytotoxic T lymphocyte lytic granule exocytosis during target cell killing, Immunity 15 (2001) 847–859.
[27] A.T. Pores-Fernando, A. Zweifach, Calcium influx and signaling in cytotoxic T-lymphocyte lytic granule exocytosis, Immunol. Rev. 231 (2009) 160–173.
[28] A. Maul-Pavicic, S.C. Chiang, A. Rensing-Ehl, B. Jessen, C. Fauriat, S.M. Wood, S. Sjoqvist, M. Hufnagel, I. Schulze, T. Bass, W.W. Schamel, S. Fuchs, H. Pircher, C.A. McCarl, K. Mikoshiba, K. Schwarz, S. Feske, Y.T. Bryceson, S. Ehl, ORAI1-mediated calcium influx is required for human cytotoxic lymphocyte degranulation and target cell lysis, Proc. Natl. Acad. Sci. U. S. A. 108 (2011) 3324–3329.
[29] I. Voskoboinik, M.C. Thia, J. Fletcher, A. Ciccone, K. Browne, M.J. Smyth, J.A. Trapani, Calcium-dependent plasma membrane binding and cell lysis by perforin are mediated through its C2 domain: a critical role for aspartate residues 429, 435, 483, and 485 but not 491, J. Biol. Chem. 280 (2005) 8426–8434.
[30] C. Weidinger, P.J. Shaw, S. Feske, STIM1 and STIM2-mediated Ca(2+) influx regulates antitumour immunity by CD8(+) T cells, EMBO Mol. Med. 5 (2013) 1311–1321.
[31] E.C. Schwarz, B. Qu, M. Hoth, Calcium, cancer and killing: the role of calcium in killing cancer cells by cytotoxic T lymphocytes and natural killer cells, Biochim. Biophys. Acta 1833 (2013) 1603–1611.
[32] A. Quintana, E.C. Schwarz, C. Schwindling, P. Lipp, L. Kaestner, M. Hoth, Sustained activity of calcium release-activated calcium channels requires translocation of mitochondria to the plasma membrane, J. Biol. Chem. 281 (2006) 40302–40309.
[33] M. Peglow, B.A. Niemeyer, M. Hoth, H. Rieger, Interplay of channels, pumps and organelle location in calcium microdomain formation, New J. Phys. 15 (2013).
[34] X. Liu, D. Weaver, O. Shirihai, G. Hajnoczky, Mitochondrial 'kiss-and-run': interplay between mitochondrial motility and fusion-fission dynamics, EMBO J. 28 (2009) 3074–3089.
[35] M. Yi, D. Weaver, G. Hajnoczky, Control of mitochondrial motility and distribution by the calcium signal: a homeostatic circuit, J. Cell Biol. 167 (2004) 661–672.
[36] M.I. Lioudyno, J.A. Kozak, A. Penna, O. Safrina, S.L. Zhang, D. Sen, J. Roos, K.A. Stauderman, M.D. Cahalan, Orai1 and STIM1 move to the immunological synapse and are up-regulated during T cell activation, Proc. Natl. Acad. Sci. U. S. A. 105 (2008) 2011–2016.
[37] J.W. Putney Jr., A model for receptor-regulated calcium entry, Cell Calcium 7 (1986) 1–12.
[38] G.W. De Young, J. Keizer, A single-pool inositol 1,4,5-trisphosphate-receptor-based model for agonist-stimulated oscillations in Ca2+ concentration, Proc. Natl. Acad. Sci. U. S. A. 89 (1992) 9895–9899.
[39] K. Samanta, P. Kar, G.R. Mirams, A.B. Parekh, Ca(2+) channel re-localization to plasma-membrane microdomains strengthens activation of Ca(2+)-dependent nuclear gene expression, Cell Rep. 12 (2015) 203–216.
[40] M.F. Ritchie, E. Samakai, J. Soboloff, STIM1 is required for attenuation of PMCA-mediated Ca(2+) clearance during T-cell activation, EMBO J. 31 (2012) 1123–1133.
[41] D.M. Bautista, M. Hoth, R.S. Lewis, Enhancement of calcium signalling dynamics and stability by delayed modulation of the plasma-membrane calcium-ATPase in human T cells, J. Physiol. 541 (2002) 877–894.
[42] M. Hoth, D.C. Button, R.S. Lewis, Mitochondrial control of calcium-channel gating: a mechanism for sustained signaling and transcriptional activation in T lymphocytes, Proc. Natl. Acad. Sci. U. S. A. 97 (2000) 10607–10612.
[43] C. Schmeitz, E.A. Hernandez-Vargas, R. Fliegert, A.H. Guse, M. Meyer-Hermann, A mathematical model of T lymphocyte calcium dynamics derived from single transmembrane protein properties, Front. Immunol. 4 (2013) 277.
[44] N.L. Allbritton, T. Meyer, L. Stryer, Range of messenger action of calcium ion and inositol 1,4,5-trisphosphate, Science 258 (1992) 1812–1815.
[45] Z. Zhou, E. Neher, Mobile and immobile calcium buffers in bovine adrenal chromaffin cells, J. Physiol. 469 (1993) 245–273.

Please cite this article in press as: I. Maccari, et al., Cytoskeleton rotation relocates mitochondria to the immunological synapse and increases calcium signals, Cell Calcium (2016), http://dx.doi.org/10.1016/j.ceca.2016.06.007

[46] M. Falcke, Reading the patterns in living cells—the physics of Ca2+ signaling, Adv. Phys. 53 (2004) 255–440.
[47] S. Means, A.J. Smith, J. Shepherd, J. Shadid, J. Fowler, R.J.H. Wojcikiewicz, T. Mazel, G.D. Smith, B.S. Wilson, Reaction diffusion modeling of calcium dynamics with realistic ER geometry, Biophys. J. 91 (2006) 537–557.
[48] R.K. Dash, F. Qi, D.A. Beard, A biophysically based mathematical model for the kinetics of mitochondrial calcium uniporter, Biophys. J. 96 (2009) 1318–1332.
[49] C. Kummerow, E.C. Schwarz, B. Bufe, F. Zufall, M. Hoth, B. Qu, A simple economic, time-resolved killing assay, Eur. J. Immunol. 44 (2014) 1870–1872.

Please cite this article in press as: I. Maccari, et al., Cytoskeleton rotation relocates mitochondria to the immunological synapse and increases calcium signals, Cell Calcium (2016), http://dx.doi.org/10.1016/j.ceca.2016.06.007